Opto-Electronics Review

Analysis of the impact of post-process modifications on the properties of TiO₂ thin films with high-temperature stable anatase phase deposited by the electron beam evaporation method

Agata Obstarczyk*⊙, Ewa Mańkowska⊙, Wiktoria Weichbrodt⊙, Paulina Kapuścik⊙, Wojciech Kijaszek⊙, Michał Mazur⊙

Faculty of Electronics, Photonics and Microsystems, Wroclaw University of Science & Technology, ul. Janiszewskiego 11/17, 50-372 Wroclaw, Poland

Article info	Abstract
	The paper describes the structural, optical, tribological, and mechanical properties of as-prepared and annealed titanium dioxide (TiO₂) coatings. TiO₂ films were deposited by the electron beam evaporation (EBE) and additionally annealed at a temperature up to 800 °C using a tubular furnace. X-ray diffraction (XRD) analysis identified the amorphous phase of coatings as-prepared and annealed at 200 °C. The phase transition to anatase occurred at 400 °C, while annealing at 600 °C and 800 °C did not induce a phase transition to the rutile phase. The crystallite size increased with an annealing up to 40.4 nm at 800 °C. Raman spectroscopy confirmed the anatase phase in thin films annealed at 400 °C and above. A scanning electron microscope (SEM) images revealed surface morphology and grain structure changes after post-process high-temperature annealing. The optical transmission measurements showed a redshift in the fundamental absorption edge with increasing annealing temperature, accompanied by a decreased transparency level. The value of an optical band gap energy (E_g^{opt}) decreased to 2.77 eV for films annealed at 800 °C. Tribological tests revealed reduced scratch resistance with higher annealing temperatures, which was attributed to increased surface roughness and coating removal. Nanoindentation measurements showed a decrease in hardness with annealing temperature, attributed to changes in crystallite size and surface morphology. This comprehensive analysis of TiO₂ thin-film coatings showed that the post-process annealing should be carefully controlled for films used in optoelectronic applications.

1. Introduction

The easiest way to transform a solid material into a vapor state is through thermal evaporation (e.g., resistive, using an electron or laser beam). Material molecules in the vapor move in the vacuum towards substrates where thin-film condensation and nucleation occur. Beside resistive heaters, an electron beam is often employed to evaporate material placed in a crucible. The properties of prepared coatings by thermal evaporation, especially mechanical and tribological, are generally poor. For instance, such thin films typically exhibit low hardness, poor wear resistance, and weak adhesion to substrates. To improve the properties of coatings deposited by evaporation, increasing the total energy of material reaching the substrates is necessary. This energy is the sum of all factors contributing to the potential and kinetic energy of the nucleating particle on a substrate. In practice, methods to increase the energy of nucleating particles include, among others, additional heating of the substrates, reducing the pressure in the working chamber, applying additional electrical potential to the substrates, or using ion beam assistance to provide better quality coatings with high adhesion to the substrate [1].

*Corresponding author at: agata.obstarczyk@pwr.edu.pl

The electron beam evaporation (EBE) process is a kind of physical vapor deposition (PVD) that provides a rapid deposition rate achieved at comparatively low substrate temperatures. This process provides numerous opportunities for controlling the structure and morphology of coatings to achieve specific properties, including densely packed coatings, excellent thermal efficiency, minimal contamination, and high reliability and productivity. Moreover, the EBE method provides easy control and excellent cost-effectiveness [2–7].

One of the most common post-processing modifications of the properties of thin films is their annealing. Post-process annealing of thin films can affect, among others, the increase of crystallite size, changes in the stresses in the coating structure, transitions in the type of crystal structure, and modifications to the surface morphology [1, 3, 8, 9]. The impact on the modification of the mentioned parameters is not only determined by the final annealing temperature but also by the annealing time, the rate of heating and cooling during annealing, and the type of gas atmosphere [5]. Nevertheless, a significant drawback of the annealing is the side effect related to grain size increase and surface chemical state changes [10].

Recently, there has been growing interest in applying titania oxide coatings. Titanium dioxide (TiO_2) can be found in an amorphous form and as orthorhombic brookite and tetragonal anatase or rutile. However, the rutile phase is thermodynamically stable at higher temperatures [11–13]. A proper crystal structure is often essential for developing devices with desired and specialized performance parameters. It is widely known that controlling the crystalline phase of TiO_2 coatings, both in the as-prepared and after post-process annealing, is crucial. However, depending on the deposition method and growth conditions, crystalline or amorphous TiO_2 films can be obtained [11, 14, 15]. Titania coatings deposited by the method at low growth temperatures are often amorphous [16]. Post-process modification like annealing is usually used to crystalize the as-prepared coatings, improving their crystallinity and multifunctional properties [10]. The anatase phase of TiO_2 predominates in coatings prepared at lower growth temperatures, such as EBE. However, when the growth temperature exceeds 600 °C, the stable rutile phase appears [13, 17]. According to Ref. 18, TiO_2 with an anatase phase is considered the most photoactive and practical among semiconductors for various environmental applications. Some reports indicate that under certain conditions, the rutile phase of TiO_2 exhibits higher photocatalytic activity. Additionally, in some cases, a mixture of these two phases proves more efficient, possessing properties not observed in either phase [18]. Furthermore, subjecting anatase-TiO_2 to additional annealing exceeding 700 °C results in a phase transition to the rutile [19–22]. However, Taherniya *et al.* [12] reported that as-deposited TiO_2 films prepared by the EBE method started to crystallize above 450 °C into the tetragonal anatase phase. Wong *et al.* [23] prepared TiO_2 coatings using the sol-gel method, and they noted an increase in the crystallite size and surface roughness of the prepared films with an increase in temperature. Furthermore, Lin *et al.* [24] investigated the influence of annealing temperature on the structure, morphology, and optical characteristics of TiO_2 coatings deposited through spin coating. Their findings indicated that phase transition from amorphous to anatase-

TiO_2 occurred at 400 °C, with a simultaneous reduction in the bandgap. Metal cations can be applied to dop TiO_2 to enhance the stability of the high-temperature anatase phase. However, several articles have been published over the years on extending the temperature range of the phase transition from anatase to rutile through non-metal doping of titania oxide [25]. Stable at high temperatures, antimicrobial anatase offers the advantage of applying to products processed at higher temperatures within the 650–1100 °C range, such as bathroom fittings. Applying TiO_2 during manufacturing can transform it into the non-photocatalytically active rutile phase. A method for preparing a stable anatase phase at high temperatures is needed to overcome this. Developing a synthesis technique that retains the photocatalytically active high-temperature stable anatase phase allows the production of self-cleaning building materials with minimal modifications to existing manufacturing techniques [25].

It is challenging to find reports in the literature regarding a high-temperature stable anatase phase in coatings prepared by the EBE method [12, 26]. This study aimed to analyse the structural, optical, tribological, and mechanical properties of TiO_2 deposited and annealed via EBE.

2. Experimental

TiO_2 coatings were prepared using the EBE method. During deposition, Ti_3O_5 pellets (99.99 at.% purity) were evaporated from a tungsten boat for 60 min. The base pressure was kept below $1.7 \cdot 10^{-3}$ mbar and thin films were deposited under oxygen atmosphere with a total gas flow of 100 sscm. The distance between the tungsten boat and the substrates (SiO_2, silicon, and TiAlV alloy) was about 500 mm. Before the EBE processes, plasma cleaning of the working chamber and deposition substrates was carried out. The substrates were rotated at 3 rpm to obtain homogeneous coatings. Ti oxide films were deposited without additional ion-beam assistance, and the current was 150 mA. Moreover, the EBE process was monitored by a thickness sensor. Silica and silicon substrates were chosen to evaluate the prepared coatings structural properties and surface morphology. However, SiO_2 and TiAlV substrates were used to determine optical and mechanical properties. The thickness of as-deposited coatings was examined using an optical profilometer (Talysurf CCI Lite) equalling 320 nm. After the EBE process, TiO_2 films were annealed using a quartz tube in a Nabertherm tubular furnace. To precisely determine the post-process modification, TiO_2 coatings were annealed at 200 °C, 400 °C, 600 °C, and 800 °C for 2 h in an ambient atmosphere, with a heating curve of 200 °C per hour. After this time, the furnace was cooled down to ambient temperature without refrigerant flow, additional ventilation, or liquid nitrogen.

Structural properties were analysed using Raman spectroscopy and X-ray diffraction (XRD). Raman spectroscopy measurements were conducted using a Thermo Fisher Scientific Raman Microscope. A PANalytical Empyrean powder diffractometer was used to carry out XRD measurements. According to Debye-Scherrer's equation [27], the average crystallite size was calculated using MDI Jade 5.0 software.

The optical properties, such as the fundamental absorption edge (λ_{cutoff}) and optical band gap energy (E_g^{opt}),

were determined based on the light transmission spectra. The measurements were conducted using an Ocean Optics QE 65 000 spectrophotometer.

Surface morphology and cross-section of as-prepared and annealed coatings were examined with the use of a scanning electron microscope (SEM) FEI Nova NanoSEM 230, using a secondary electron detector. The hardness and Young's modulus of as-prepared and annealed TiO_2 films were determined using the nano-indentation technique. Nanoindentation measurements were conducted using a CSM Instruments nanoidenter fitted with a Vickers indenter tip, employing the Oliver and Pharr method [28–30].

The protective characteristics of the as-prepared and annealed coatings were examined using specialized measurement equipment from Summers Optical's Lens Coating Hardness Test Kit, which is used, among other purposes, for testing the abrasion resistance of coatings on optical lenses. This equipment is employed for coating measurements under U.S. military standards (MIL-C-00675, MIL-M-13508, and MIL-F-48616). The abrasion resistance of various coatings is determined based on a steel wool test, corresponding to ISO standards [31]. The steel wool test consisted of rubbing the surface of as-deposited and annealed coatings for 75 cycles with a 0-grade steel wool pad using an applied load of 1.0 N. Before and after steel wool tests, the surface of coatings was examined by an optical microscope (Olympus BX51) and an optical profilometer (TalySurf CCI Lite Taylor Hobson).

3. Results and discussion

Based on the obtained diffractograms (Fig. 1), it was found that as-prepared and annealed at 200 °C TiO_2 films were amorphous. Only broad, amorphous-like patterns without peaks related to the anatase or rutile phases were visible. According to our previous works [30], the amorphous microstructure of as-deposited TiO_2 coating resulted from the deposition process. EBE is a low-temperature process with low energy of evaporated ions. Further annealing of TiO_2 films at 400 °C and 600 °C caused phase transition with peaks related to a tetragonal phase of TiO_2-anatase. Based on the data contained in the powder diffraction file PDF (21-1272) [32], all peak positions of TiO_2 coating correspond to the anatase phase. The peak intensity from the (004) crystal plane is the strongest for the film annealed at 800 °C [Fig. 1(a)].

Further annealing of TiO_2 coating at 800 °C did not lead to the phase transition from the anatase to rutile phase or into the mix of anatase-rutile phases. Other research has shown that the irreversible phase transformation from anatase to rutile occurs at temperatures between 450 °C and 850 °C and it is related to the preparation method and precursors used in process deposition [20, 33–36]. Zhang et al. [37] mentioned a few reports on successfully preparing TiO_2 films with a pure anatase phase stable at high temperatures above 900 °C. Moreover, they reported that the anatase phase of TiO_2 coatings with high thermal stability until 1000 °C were prepared by mist chemical vapor deposition. According to Ref. 38, the XRD patterns for an annealing temperature of 300 °C do not show any peak, which indicates that the TiO_2 films were amorphous. Rahmahwati et al. [38] also mentioned that to obtain TiO_2 with anatase phase, a high-temperature calcination, at least at 400 °C, is required. However, an irreversible phase transformation to rutile was observed at higher temperatures between 600 °C and 800 °C. Zenkovets et al. [39] obtained thermally stable TiO_2-anatase nanocomposites doped with cerium or yttrium elements. All dopants used in this research stabilized anatase phase up to 900 °C [39]. Moreover, Scherrer's formula was used to calculate the average crystallite size [27]. The crystallite size for modified coatings at 400 °C, 600 °C, and 800 °C was calculated considering the most dominant peak for (004) lattice plane, which occurred at $2\theta = 38°$. In the case of film annealed at 400 °C, the crystallites had the size of ca. 14.4 nm. The diffraction peaks become more intense for the coatings annealed at higher temperatures. XRD studies also revealed that a further increase in temperature of post-process annealing leads to an increase in crystallite size to ca. 19.8 nm and 40.4 nm for films annealed at 600 °C and 800°C, respectively [Fig. 1(b)]. Taherniya et al. [12] described that the initial crystallization temperature from the amorphous to the anatase phase of TiO_2 coatings occurred at 450 °C. Moreover, the crystallite size of the thin films increases up to 24 nm with an increase in the annealing temperature to 600 °C. Miller et al. [40] also found that annealing TiO_2 films at 450 °C is sufficient to initiate a phase transformation from an amorphous to a crystalline TiO_2 coating. Nair et al. [41] also reported that the initial temperature of crystallization of TiO_2 film can equal 300 °C [41]. Moreover, the type of stress occurring in the annealed coatings was determined based on Δd parameter [42–44]. This parameter represents the relative difference between the measured interplanar distance and
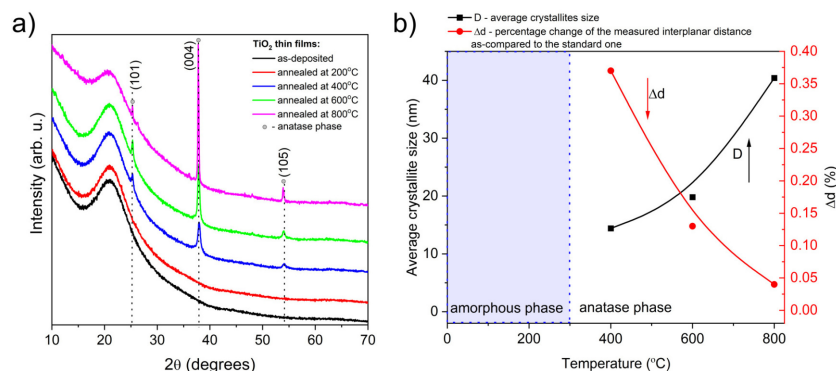

Fig. 1. Structural properties of as-prepared and annealed TiO_2 coatings deposited by the EBE method: (a) XRD patterns and (b) the dependence of average crystallites size and Δd parameter on annealing temperature

the standard value. The compressive stresses occur in the coatings if Δd parameter is lower than zero. However, when Δd value is higher than zero, tensile stress is observed. For annealed coatings, the XRD analysis showed a slight shift in the measured diffraction peaks toward higher angles, while also indicating the presence of compressive stresses. With the annealing temperature increase to 800 °C, the compressive stress was almost ten times lower compared to coating with the anatase phase annealed at 400 °C [Fig. 1(b)]. The results of the XRD measurements are summarized in Table 1.

Raman spectroscopy was used to investigate the microstructure of as-prepared and annealed TiO_2 coatings. According to Refs. 45–47, TiO_2 exists in three natural forms like anatase, rutile, and brookite. Anatase and rutile phase are tetragonal and have six and four Raman active modes, respectively. Meanwhile, brookite (orthorhombic) has 36 Raman active modes [45–48]. Figure 2(a) and (b) showed Raman spectra of as-prepared and annealed TiO_2 coatings. The results obtained by Raman spectroscopy are consistent with the reference values for anatase phases [48] for coatings after post-process modification at 400 °C, 600 °C, and 800 °C, while as-prepared and annealed TiO_2 film at 200 °C showed amorphous phase. The results obtained are consistent with those of the XRD studies. The typical Raman peaks observed at ca. 395 cm^{-1}, 516 cm^{-1}, and 636 cm^{-1} [Fig. 2(b)] suggest that the microstructure of annealed films at 400 °C and 600 °C is composed of the anatase phase. It is worth noting that an additional peak related to the anatase phase occurring at 195 cm^{-1} was observed for films annealed at 800 °C [Fig. 2(a)]. Moreover, the intensity of these peaks indicates the presence

of a highly crystalline TiO_2 structure after the annealing process. Furthermore, vibrational modes of the TiO_2-rutile phase were not observed. Raman spectra presented in Fig. 2(a) and (b) are consistent with reference values and slightly shifted due to the instrumental error bar [29].

SEM images of as-prepared and annealed at 200 °C and 400 °C TiO_2 coatings [Fig. 3(a)–(c)] showed a columnar-like character, with a surface composed of very small, densely packed grains. Post-process annealing at 600 °C resulted in a similar cross-section to as-prepared films and a noticeable increase of grains and small voids between them. TiO_2 film annealed at the highest temperature (800 °C) had milky colour, related to the morphology change from densely packed fibrous-like to the coarse grain-type. Furthermore, Rahmahwati *et al.* [38] and Shailesh *et al.* [49] reported that higher post-process annealing led to a breakdown of larger crystallites into smaller ones, forming conglomerates that resulted in coating cracking [Fig. 3(e)].

Figure 4(a) shows the optical properties of as-prepared and annealed TiO_2 coatings. For an as-prepared and annealed at 200 °C amorphous-TiO_2 thin film, the cut-off wavelength (λ_{cutoff}) was equal to 326 nm and 328 nm, respectively. After post-process annealing at 400 °C and 600 °C, only a slight redshift of the λ_{cutoff} was observed [Fig. 4(a)]. The transparency level (T_λ) for prepared and annealed coatings from 200 °C to 600 °C was very similar, ca. 77%. On the other hand, the high temperature of post-annealing (800 °C) led to a decrease of the T_λ to ca. 44%, resulting in a milky coating colour due to the morphology change. In the case of the anatase film annealed at 800 °C, a redshift in λ_{cutoff} from 326 nm to 337 nm was observed for

Table 1.
Results of the XRD measurements.

| TiO_2 thin film	Phase	Crystal plane	D (nm)	d (nm)	d_{PDF} (nm)	Δd (%)	Type of stress
as-prepared	amorphous	–	–	–		–	–
annealed 200 °C		–	–	–		–	–
annealed 400 °C		(004)	14.4	0.2369		−0.37	compressive
annealed 600 °C	TiO_2-anatase	(004)	19.8	0.2375	0.2378 [32]	−0.13	compressive
annealed 800 °C		(004)	40.4	0.2377		−0.04	compressive
Designations: D – calculated average crystallite size according to the Scherrer's equation [27]; d – measured interplanar distance; Δd – percentage change of the measured interplanar distance as-compared to the standard one (d_{PDF}) [32].							
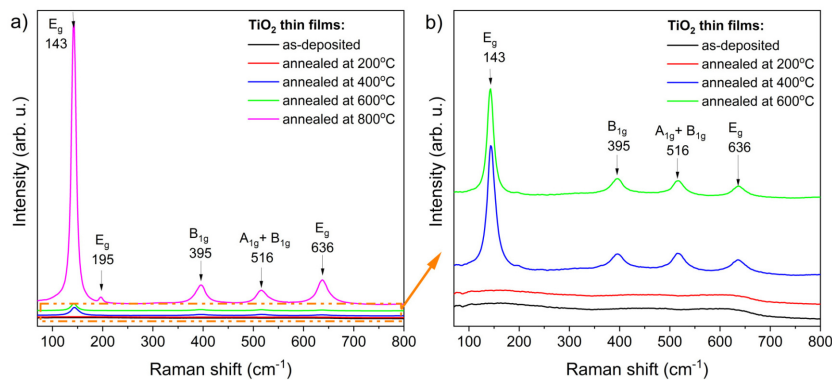
Fig. 2. Raman spectra of: (a) as-prepared and annealed TiO_2 coatings deposited by EBE method and (b) magnification of Raman spectra for as-prepared and annealed coatings from 200 °C to 600 °C as the peaks were much less intense than TiO_2 annealed at 800 °C.
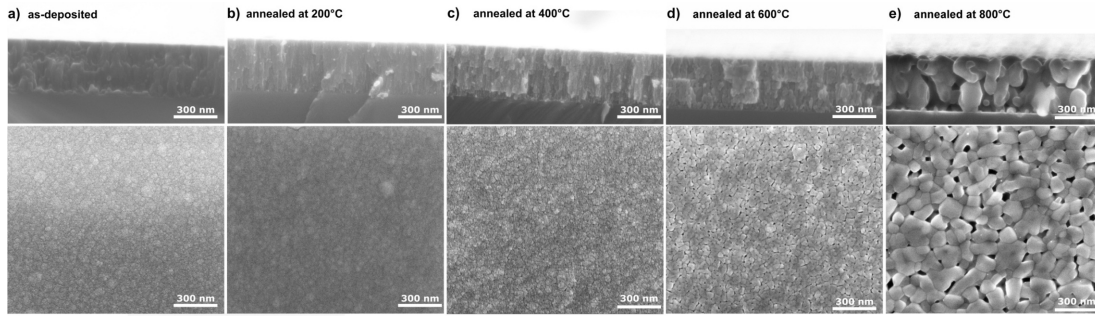
Fig. 3. SEM images of the cross-section and surface of (a) as-prepared and annealed TiO₂ coatings and at: (b) 200 °C, (c) 400 °C, (d) 600 °C, and (e) 800 °C deposited by EBE method.
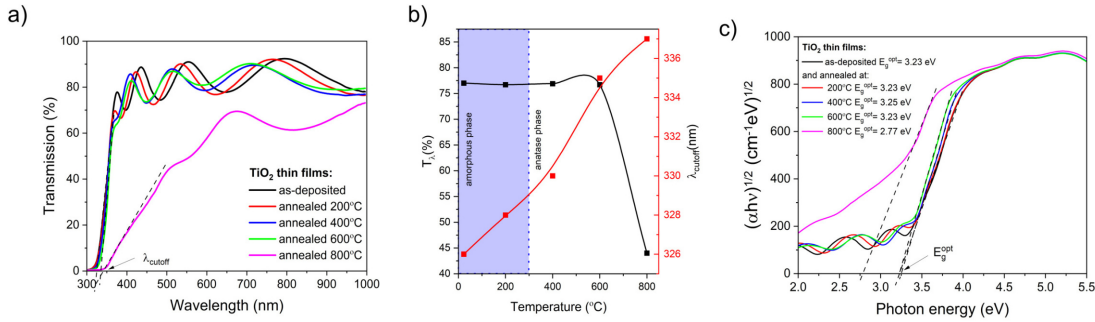

Fig. 4. Optical properties of TiO₂ coatings prepared by EBE method: (a) transmittance spectra with marked λ_{cutoff}, (b) transparency level (T_λ), and fundamental absorption edge as a function of annealing temperature and (c) E_g^{opt} in the function of photon energy.

as-prepared and annealed films. The dependence between the transparency level and the fundamental absorption edge as a function of annealing temperature reveals changes in TiO₂ coatings [Fig. 4(b)].

According to Taherniya *et al*. [12], the as-deposited TiO₂ films with the amorphous phase deposited by the EBE method obtain crystallinity anatase phase after post-process annealing. However, post-process modification can cause opacity and optical transmittance to decrease with the increase of annealing temperature from ca. 90% to 82% for as-prepared and annealed films at 600 °C, respectively [12, 50]. Due to a lower light scattering effect of the film surface, an average transmittance spectrum of as-prepared TiO₂ coatings in the visible region was more than 80%, as reported by Refs. 11, 12, 51, and 52.

According to Refs. 11 and 21, TiO₂ is an indirect band gap semiconductor. E_g^{opt} can be estimated by extrapolating the linear portion of the curves [Fig. 4(c)] [48]. For as-prepared and annealed coatings from 200 ° to 600 °C, the E_g^{opt} was ca. 3.20 eV. For TiO₂ annealed at 800 °C, the decrease of the E_g^{opt} to 2.77 eV, was observed. According to Pjević *et al*. [18], a decrease in the E_g with increasing annealing temperature is due to decreasing interatomic spacing (amorphous-crystalline), removal of defects, and increasing the size of crystalline grains. Moreover, Reference 11 reported that the indirect optical band gap of the TiO₂ coatings with anatase structure was in the range of 3.39–3.42 eV, respectively, as the substrate temperature increased. Table 2 summarizes the analysis of the optical parameters.

In the case of TiO₂ coatings with highly stable anatase phases, which may find applications in optoelectronics or as corrosion-protective coatings on metals, their tribological properties are significant. For as-deposited and annealed

Table 2.
Optical parameters of as-prepared and annealed TiO₂ coatings prepared by the EBE method.

TiO₂ thin film	Phase	T_λ (%)	λ_{cutoff} (nm)	E_g^{opt} (eV)
as-deposited	amorphous	77.0	326	3.23
annealed 200 °C		76.7	328	3.23
annealed 400 °C	TiO₂-anatase	76.9	330	3.25
annealed 600 °C		76.7	335	3.23
annealed 800 °C		44.4	337	2.77

coatings up to 600 °C before the abrasion test (Fig. 5 to Fig. 8), their surface was smooth, homogenous, and without scratches. The root mean square height (S_q) parameter was approximately 0.90 nm, for as-prepared and annealed coatings up to 600 °C. For coating annealed at 800 °C, the S_q value increased to 2.43 nm before the scratch test (Fig. 9, left side). Additionally, images of the surface obtained with an optical microscope showed grains without visible cracks. After the abrasion test, it can be concluded that annealed coatings up to 800 °C did not protect against scratches. The S_q parameter increased significantly up to 145 nm for coating after post-process annealing at 600 °C due to a visible surface damage. However, the S_q value of the coating annealed at the highest temperature (800 °C) was 2.29 nm. Based on Fig. 9 (right side), it can be stated that the TiO₂ coating was completely removed from the substrate (Fig. 9, right side). Furthermore, Figures from 5 to 9 showed a comparison of surface cross-sectional profiles of the as-prepared and annealed films before and after the scratch test. In the case of as-prepared and annealed coatings up to 600 °C, it was observed that after the steel wool test, the surface of the coatings was signifi-
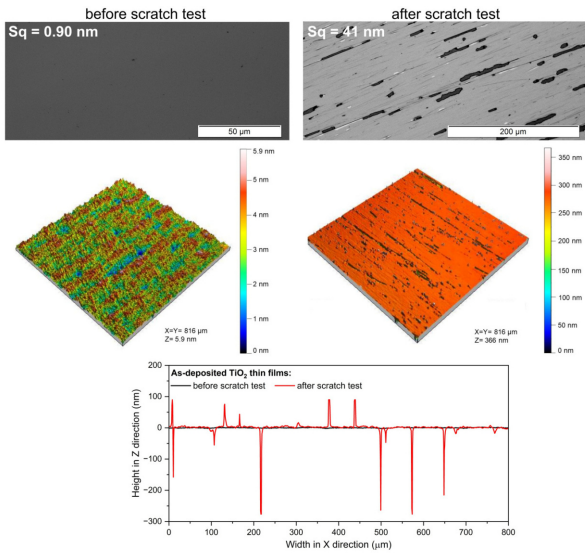
Fig. 5. Surface topography profiles for as-deposited TiO$_2$ coatings prepared by the EBE method.
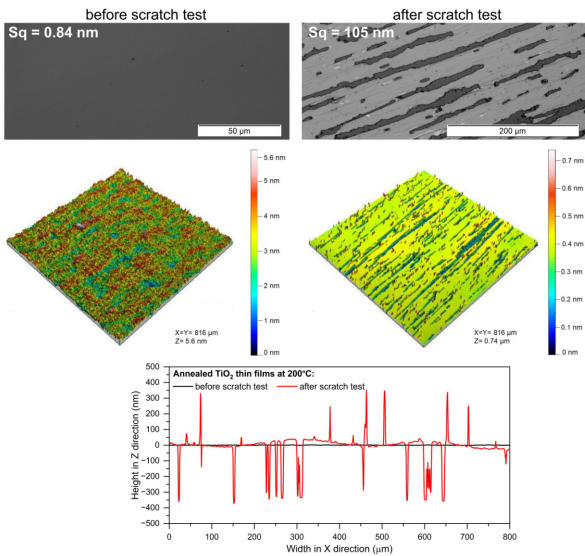
cantly damaged, with the maximum depth of scratches achieving more than 300 nm. For anatase coatings after post-process annealing at 800 °C, the cross-sectional profile was similar to that before the test because the coatings after the abrasion test were almost completely removed from the substrate, forming a substrate-derived profile (Fig. 9).

The hardness of the as-prepared and annealed TiO$_2$ coatings was measured based on the nanoindentation and approximation method. The surface hardness obtained for as-deposited amorphous-TiO$_2$ was equal to 5.1 GPa [Fig. 10(a)]. After annealing at 200 °C, the hardness of TiO$_2$ coating decreased to 4.4 GPa [Fig. 10(b)]. An increase in annealing temperature to 400 °C and due to the change of microstructure from amorphous to anatase phase, the hardness increased to 5.7 GPa [Fig. 10(c)]. According to Gao *et al*. [53], materials with an amorphous phase show a tendency towards lower hardness than materials with a nanocrystalline structure. A further decrease in hardness for coatings annealed at 600 °C and 800 °C was observed to 3.0 GPa and 2.0 GPa, respectively [Fig. 10(d), and (e)].
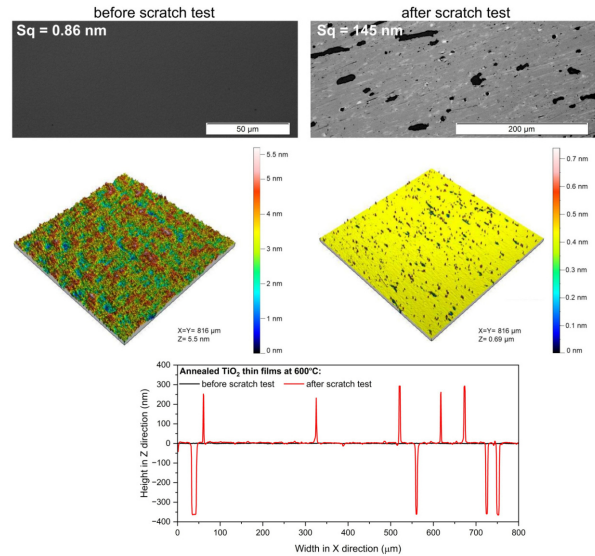

Fig. 6. Surface topography profiles for TiO$_2$ coatings prepared by the EBE method after annealing at 200 °C.

Fig. 8. Surface topography profiles for TiO$_2$ coatings prepared by the EBE method after annealing at 600 °C.

Fig. 7. Surface topography profiles for TiO$_2$ coatings prepared by the EBE method after annealing at 400 °C.
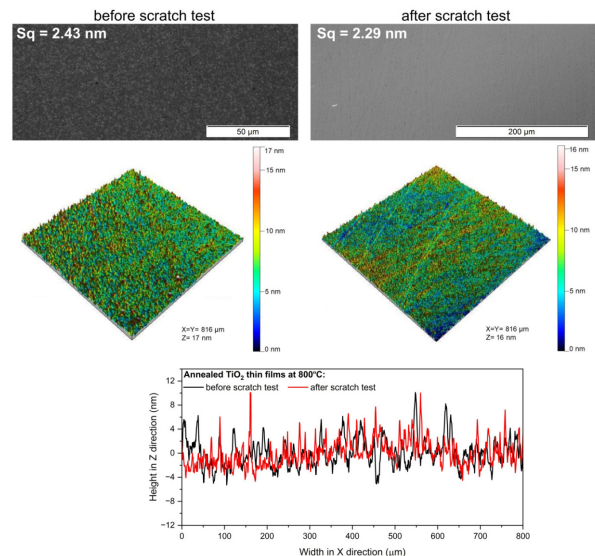

Fig. 9. Surface topography profiles for TiO$_2$ coatings prepared by the EBE method after annealing at 800 °C.
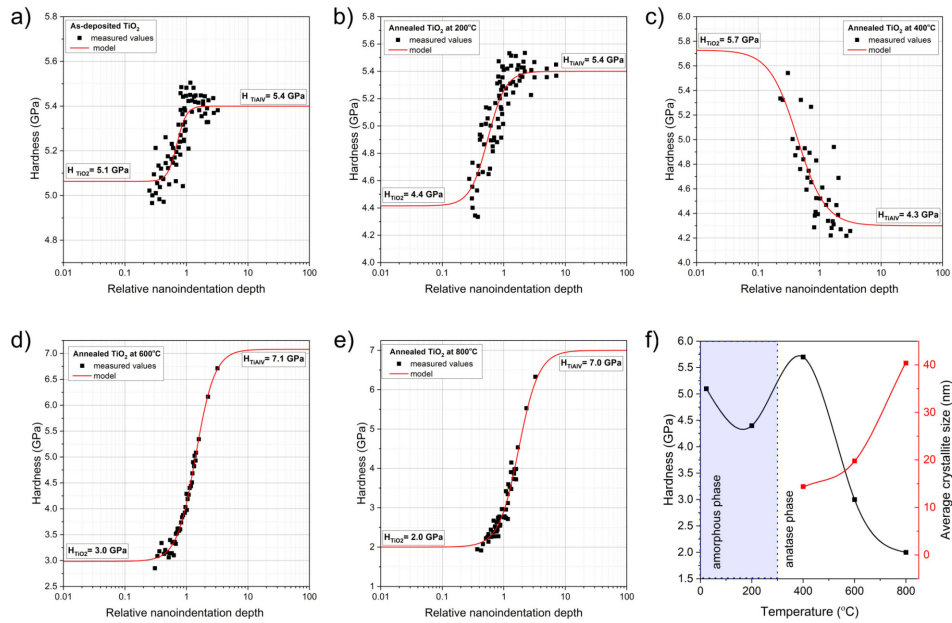
Fig. 10. Results of hardness of (a-e) as-prepared and annealed TiO$_2$ coatings deposited by EBE method and (f) Hall-Petch effect of TiO$_2$ coatings.

However, in the case of nanocrystalline TiO$_2$ films, the mechanical parameters deteriorate after post-process annealing. The large hardness difference between as-deposited and annealed films can be related to the difference in crystallite size and surface morphology. Based on the Hall-Petch effect, the hardness of the material increases with the grain size decrease [53] [Fig. 10(f)]. In the case of coatings after post-process modification at 400 °C, 600 °C, and 800 °C after microstructure changes, the crystallite size increased from 14.4 nm to 19.8 nm and 40.4 nm, respectively. This can result in a decrease in the hardness of this film due to significant differences in the crystallite size, thus causing a decrease in hardness from 5.7 GPa to 3.0 GPa and 2.0 GPa. The results showed that post-process annealing may possibly have a detrimental effect on the mechanical and tribological properties of prepared coatings. Due to this knowledge, post-process modification should be monitored and controlled carefully because TiO$_2$ thin films are often used in optical devices [40].

4. Conclusions

In this paper, the EBE method prepared TiO$_2$ coatings with a high-temperature stable anatase phase. The post-process modification of as-prepared coatings was conducted with the precisely determined annealing temperature up to 800 °C. XRD studies revealed that as-prepared and annealed at 200 °C TiO$_2$ films were amorphous. Further annealing at higher temperatures caused crystallization with peaks related to the TiO$_2$-anatase phase. The phase transition from anatase to rutile or a mixture of these phases system was not observed even at the highest annealing temperature, i.e., 800 °C. Additionally, the Raman spectroscopy confirmed that the as-prepared and annealed at 200 °C films were amorphous, while the anatase phase was observed for films annealed at higher temperatures. Scanning electron microscopy revealed changes in surface morphology with increasing annealing temperature, including grain growth and the formation of voids. The optical results indicated that amorphous and annealed coatings from 200 °C to 600 °C were transparent with an average transmission of ca. 77%. After post-process annealing at 400 °C and 600 °C, optical transmission measurements showed a redshift in the absorption edge, indicating phase change. However, the transparency level decreased with higher annealing temperatures to 44% for 800 °C. The E_g^{opt} decreased with annealing, which was related to the significant increase in crystallite size and presence of defects. The post-process annealing affected the tribological properties and hardness of thin films. Tribological testing revealed a decreased scratch resistance with higher annealing temperatures along with changes in the surface hardness. Nanoindentation measurements revealed a decrease in hardness with annealing due to the changes in the microstructure and crystallite size. The hardness of as-deposited amorphous-TiO$_2$ was equal to 5.1 GPa. After post-process modification at 200 °C, the hardness decreased to 4.4 GPa. Further, annealing at 400 °C resulted in a phase change to anatase, increasing the hardness to 5.7 GPa. However, annealing at 600 °C and 800 °C decreased hardness values to 3.0 GPa and 2.0 GPa, respectively. This deterioration in mechanical properties contradicts the expected trend, possibly due to changes in crystallite size and surface morphology. Moreover, the increase in crystallite size (from 14.4 nm to 40.4 nm) with annealing temperature was observed.

To conclude, post-process modification, like annealing, significantly influenced the structural, optical, mechanical, and tribological properties of TiO$_2$ coatings. Ti-oxide coatings with a highly stable anatase phase, which may have applications in optoelectronics or as corrosion-protective coatings, are critical in terms of their tribological properties. These findings emphasize the necessity of precise control over annealing processes to maintain desired mechanical properties, particularly for TiO$_2$ coatings used in optical devices.

Declaration of competing interest

The authors declare that they have no conflicts of interest with this work.

Authors' statement

Conceptualization, data curation, formal analysis, investigation, methodology, visualization, writing original draft, writing review & editing, A.O.; investigation, methodology, visualization, E.M.; investigation, W.W., W.K., and P.K.; supervision, conceptualization, formal analysis, investigation, writing original draft, writing review & editing, resources, validation, project administration, funding acquisition, M.M.

References

[1] Nagabharana, R. M., Kumaraswamy, G. N., Gundanna, S. K. & Bhatta, U. M. Effect of thermal annealing on structural and electrical properties of TiO₂ thin films. *Thin Solid Films* **710,** 138262 (2020). https://doi.org/10.1016/j.tsf.2020.138262

[2] Kerdcharoen, T. & Wongchoosuk, C. 11-Carbon Nanotube and Metal Oxide Hybrid Materials for Gas Sensing. in *Semiconductors Gas Sensors* (eds. Jaaniso, R. & Tan, O. K.) 386–407 (Woodhead Publishing Ltd., 2013). https://doi.org/10.1533/9780857098665.3.386

[3] Lu, Z., Jiang, X., Zhou, B., Wu, X. & Lu, L. Study of the effect of annealing temperature on the structure, morphology, and photocatalytic activity of Si-doped TiO₂ thin films deposited by electron beam evaporation. *Appl. Surf. Sci.* **257,** 10715–10720 (2011). https://doi.org/10.1016/j.apsusc.2011.07.085

[4] Lee, S. H. *et al*. Deposition and characterization of silicon thin film on stainless steel by electron beam evaporation. *Thin Solid Films* **756,** 139380 (2022). https://doi.org/10.1016/j.tsf.2022.139380

[5] Dey, B. *et al*. Anatase TiO₂ deposited at low temperature by pulsing an electron cyclotron wave resonance plasma source. *Sci. Rep.* **10,** 21952 (2020). https://doi.org/10.1038/s41598-020-78956-1

[6] Matkivskyi, V. *et al*. Electronic-beam evaporation processed titanium oxide as an electron selective contact for silicon solar cells. *Curr. Appl. Phys.* **32,** 98–105 (2021). https://doi.org/10.1016/j.cap.2021.10.005

[7] Bashir, A., Awan, T. I., Tehseen, A., Tahir, M. B. & Ijaz, M. Chapter 3 – Interfaces and Surfaces. in *Chemistry of Nanomaterials: Fundamentals and Applications* 51–87 (Elsevier, 2020). https://doi.org/10.1016/B978-0-12-818908-5.00003-2

[8] Mukherjee, S. K. *et al*. Influence of thickness on the structural properties of radio-frequency and direct-current magnetron sputtered TiO₂ anatase thin films. *Thin Solid Films* **558,** 443–448 (2014). https://doi.org/10.1016/j.tsf.2014.02.048

[9] Ali, S. M. & Khan, M. A. M. Annealing effects on structural, optical, and electrical properties of TiO₂/FTO heterojunction. *Appl. Phys. A* **126,** 468 (2020). https://doi.org/10.1007/s00339-020-03656-6

[10] Zhao, C., Child, D., Gibson, D., Placido, F. & Fu, R. Y. Q. TiO₂ films prepared using plasma ion assisted deposition for photocatalytic application. *Mater. Res. Bull.* **60,** 890–894 (2014). https://doi.org/10.1016/j.materresbull.2014.09.022

[11] Hasan, M. M., Haseeb, A. S. M. A., Saidur, R., Masjuki, H. H. & Hamdi, M. Influence of substrate and annealing temperatures on optical properties of RF-sputtered TiO₂ thin films. *Opt. Mater.* **32,** 690–695 (2010). https://doi.org/10.1016/j.optmat.2009.07.011

[12] Taherniya, A. & Raoufi, D. The annealing temperature dependence of anatase TiO₂ thin films prepared by the electron-beam evaporation method. *Semicond. Sci. Tech.* **31,** 125012 (2016). https://doi.org/10.1088/0268-1242/31/12/125012

[13] Kumi-Barimah, E. *et al*. Phase evolution, morphological, optical, and electrical properties of femtosecond pulsed laser-deposited TiO₂ thin films. *Sci. Rep.* **10,** 10144 (2020). https://doi.org/10.1038/s41598-020-67367-x

[14] Jolivet, A. *et al*. Structural, optical, and electrical properties of TiO₂ thin films deposited by ALD: Impact of the substrate, the deposited

[15] Bukauskas, V. *et al*. Effect of substrate temperature on the arrangement of ultra-thin TiO₂ films grown by a DC-magnetron sputtering deposition. *Thin Solid Films* **585,** 5–12 (2015). https://doi.org/10.1016/j.tsf.2015.04.007

[16] Mangrola, M .H. & Joshi, V. G. Synthesis, characterization and study of influence of pure TiO₂ nanoparticles thin film developed by e-beam evaporation. *Materials Today: Proc.* **4,** 3832–3841 (2017). https://doi.org/10.1016/j.matpr.2017.02.281

[17] Pillai, S. C. *et al*. Synthesis of high-temperature stable anatase TiO₂ photocatalyst. *J. Phys. Chem. C.* **111,** 1605–1611 (2007). https://doi.org/10.1021/jp065933h

[18] Pjević, D. *et al*. Properties of sputtered TiO₂ thin films as a function of deposition and annealing parameters. *Phys. B: Condens. Matter.* **463,** 20–25 (2015). https://doi.org/10.1016/j.physb.2015.01.037

[19] Diebold, U. The surface science of titanium dioxide. *Surf. Sci. Rep.* **48,** 53–229 (2003). https://doi.org/10.1016/S0167-5729(02)00100-0

[20] Hanaor, D. A. & Sorrell, C. C. Review of the anatase to rutile phase transformation. *J. Mater. Sci.* **46,** 855–874 (2011). https://doi.org/10.1007/s10853-010-5113-0

[21] Rahimi, N., Pax, R. A. & MacA. Gray, E. Review of functional titanium oxides. I: TiO₂ and its modifications. *Prog. Solid State Chem.* **44,** 86–105 (2016). https://doi.org/10.1016/j.progsolidstchem.2016.07.002

[22] Wen, P. C., Cai, C., Zhong, H., Hao, L. Y. & Xu, X. A simple way to synthesize anatase with high thermal stability. *J. Mater. Sci.* **50,** 5944–5951 (2015). https://doi.org/10.1007/s10853-015-9117-7

[23] Wong, A., Daoud, W. A., Liang, H. & Szeto, Y. S. The effect of aging and precursor concentration on room-temperature synthesis of nanocrystalline anatase TiO₂. *Mater. Lett.* **117,** 82–85 (2014). https://doi.org/10.1016/j.matlet.2013.11.056

[24] Lin, C. P., Chen, H., Nakaruk, A., Koshy, P. & Sorrell, C. C. Effect of annealing temperature on the photocatalytic activity of TiO₂ thin films. *Energy Procedia* **34,** 627–636 (2013). https://doi.org/10.1016/j.egypro.2013.06.794

[25] Fagan, R., Synnott, D. W., McCormack, D. E. & Pillai, S. C. An effective method for the preparation of high-temperature stable anatase TiO₂ photocatalysts. *Appl. Surf. Sci.* **371,** 447–452 (2016). https://doi.org/10.1016/j.apsusc.2016.02.235

[26] Khan, A. F., Mehmood, M., Durrani, S. K., Ali, M. L. & Rahim, N. A. Structural and optoelectronic properties of nanostructured TiO₂ thin films with annealing, *Mater. Sci. Semicond. Process.* **29,** 161–169 (2015). https://doi.org/10.1016/j.mssp.2014.02.009

[27] Klug, H. P. & Alexander, E. E. *X-Ray Diffraction Procedures for Polycrystalline and Amorphous Materials, 2nd ed.* (John Wiley and Sons, New York, 1974).

[28] Oliver, W. C. & Pharr, G. M. An improved technique for determining hardness and elastic modulus using load and displacement sensing indentation experiments. *J. Mater. Res.* **7,** 1564–1583 (1992). https://doi.org/10.1557/JMR.1992.1564

[29] Wiatrowski, A. *et al*. Comparison of the physicochemical properties of TiO₂ thin films obtained by magnetron sputtering with continuous and pulsed gas flow. *Coatings* **8,** 412 (2018). https://doi:10.3390/coatings8110412

[30] Obstarczyk, A. *et al.* Influence of post-process annealing temperature on structural, optical, mechanical, and corrosion properties of mixed TiO₂-WO₃ thin films. *Thin Solid Films* **698,** 137856 (2020). https://doi.org/10.1016/j.tsf.2020.137856

[31] ISO/TC 172/SC 7/WG 3N30 Standard, Spectacle Lenses: Test Method for Abrasion Resistance (1998). https://www.iso.org/committee/53738.html

[32] Powder Diffraction File, Joint Committee on Powder Diffraction Standards, ASTM, Philadelphia, PA, Card 21-1272 – PDF (1969). https://www.icdd.com/pdf-5/

[33] Li, J., Liu, L. & Sham, T. K. 2D XANES–XEOL Spectroscopy studies of morphology-dependent phase transformation and corresponding luminescence from hierarchical TiO₂ nanostructures. *Chem. Mater.* **27,** 3021–3029 (2015). https://doi.org/10.1021/acs.chemmater.5b00363

[34] Liu, S., Yu, J. & Jaroniec, M. Anatase TiO₂ with dominant high-energy {001} facets: Synthesis, properties, and applications. *Chem. Mater.* **23,** 4085–4093 (2011). https://doi.org/10.1021/cm200597m

[35] Garzella, C., Comini, E., Tempesti, E., Frigeri, C. & Sberveglieri, G. TiO_2 thin films by a novel sol-gel processing for gas sensor applications. *Sens. Actuators B Chem.* **68**, 189–196 (2000). https://doi.org/10.1016/S0925-4005(00)00428-7

[36] Grover, I. S., Singh, S. & Pal, B. Stable anatase TiO_2 formed by calcination of rice-like titania nanorod at 800 °C exhibits high photocatalytic activity. *RSC Adv.* **4**, 24704–24709 (2014). https://doi.org/10.1039/C4RA01850H

[37] Zhang, Q. & Li, C. High temperature stable anatase phase titanium dioxide films synthesized by mist chemical vapor deposition. *Nanomaterials* **10**, 911 (2020). https://doi.org/10.3390/nano10050911

[38] Ainuddin, A. R. & Aziz, N. A. Thermal post-treatment of TiO_2 films via sol-gel for enhanced corrosion resistance. *J. Eng. Appl. Sci.* **14** 8698–8703 (2016). https://www.arpnjournals.org/jeas/research_papers/rp_2016/jeas_0716_4663.pdf

[39] Zenkovets, G. A., Shutilov, A. A. & Gavrilov, V. Y. Heat-resistant TiO_2 nanocomposites with anatase phase as carriers for highly efficient CO oxidation catalysts. *Mater. Res. Bull.* **145**, 111538 (2022). https://doi.org/10.1016/j.materresbull.2021.111538

[40] Miller, M. J. & Wang, J. Coupled effects of deposition and annealing temperatures on optical, electrical, and mechanical properties of titanium oxide thin films. *Vacuum* **120**, 155–161 (2015). https://doi.org/10.1016/j.vacuum.2015.07.005

[41] Zhao, Z. W. & Tay, B. K. Study of nanocrystal TiO_2 thin films by thermal annealing. *J. Electroceramics* **16**, 489–943 (2006). https://doi.org/10.1007/s10832-006-9903-3

[42] Nair, P. B. *et al*. Effect of RF power and sputtering pressure on the structural and optical properties of TiO_2 thin films prepared by RF magnetron sputtering. *Appl. Surf. Sci.* **257**, 10869–10875 (2011). https://doi.org/10.1016/j.apsusc.2011.07.125

[43] Mazur, M., Kaczmarek, D., Domaradzki, J., Wojcieszak, D. & Poniedziałek, A. Influence of material composition on structural and optical properties of HfO_2-TiO_2 mixed oxide coatings. *Coatings* **6**, 13 (2016). https://doi.org/10.3390/coatings6010013

[44] Jena, S. *et al*. Effect of O_2/Ar gas flow ratio on the optical properties and mechanical stress of sputtered HfO_2 thin films. *Thin Solid Films* **592**, 135–142 (2015). https://doi.org/10.1016/j.tsf.2015.08.062

[45] Alhomoudi, I. A. & Newaz, G. Residual stresses and Raman shift relation in anatase TiO_2 thin film. *Thin Solid Films* **517**, 4372–4378 (2009). https://doi.org/10.1016/j.tsf.2009.02.141

[46] Gupta, S. K. *et al*. Synthesis, phase to phase deposition and characterization of rutile nanocrystalline titanium dioxide (TiO_2) thin films. *Appl. Surf. Sci.* **264**, 737–742 (2013). https://doi.org/10.1016/j.apsusc.2012.10.113

[47] Kadam, R. M. *et al*. Structural characterization of titania by X-ray diffraction, photoacoustic, Raman spectroscopy and electron paramagnetic resonance spectroscopy. *Spectrochim. Acta A* **137**, 363–370 (2015). https://doi.org/10.1016/j.saa.2014.08.082

[48] Nezar, S. *et al*. Properties of TiO_2 thin films deposited by rf-reactive magnetron sputtering on biased substrates. *Appl. Surf. Sci.* **395**, 172–179 (2016). https://doi.org/10.1016/j.apsusc.2016.08.125

[49] Pawar, S. *et al*. Fabrication of nanocrystaline TiO_2 thin film ammonia vapor sensor. *J. Sens. Technol.* **1**, 9–16 (2011). https://doi.org/10.4236/jst.2011.11002

[50] Vishwas, M., Narasimha Rao, K. & Chakradhar, R. P. S. Influence of annealing temperature on Raman and photoluminescence spectra of electron beam evaporated TiO_2 thin films. *Spectrochim. Acta A.* **99**, 33–36 (2012). https://doi.org/10.1016/j.saa.2012.09.009

[51] Heo, C. H., Lee, S. B. & Boo, J. H. Deposition of TiO_2 thin films using RF magnetron sputtering method and study of their surface characteristics. *Thin Solid Films* **475**, 183–188 (2005). https://doi.org/10.1016/j.tsf.2004.08.033

[52] Karuppasamy, A. & Subrahmanyam, A. Studies on the room temperature growth of nanoanatase phase TiO_2 thin films by pulsed dc magnetron with oxygen as sputter gas. *J. Appl. Phys.* **101**, 064318 (2007). https://doi.org/10.1063/1.2714770

[53] Gao, F. M. & Gao, L. H. Microscopic models of hardness. *J. Superhard Mater.* **32**, 148–166 (2010). https://doi.org/10.3103/S1063457610030020